1991年度 大韓醫用生體工學 春季 學術大會 論文集 91/5

임피던스 단층촬영기의 정적 영상 복원 알고리즘

우 응제, John G. Webster*, Willis J. Tompkins*

건국대학교 의과대학 의학공학과
* Dept. of Elec. & Comp. Eng., University of Wisconsin-Madison

A STATIC IMAGE RECONSTRUCTION ALGORITHM IN ELECTRICAL IMPEDANCE TOMOGRAPHY

Eung Je Woo, John G. Webster*, and Willis J. Tompkins*

Dept. of Biomed. Eng., Kon Kuk University
*Dept. of Elec. and Comp. Eng., University of Wisconsin-Madison

ABSTRACT

We have developed an efficient and robust image reconstruction algorithm for static impedance imaging. This improved Newton-Raphson method produced more accurate images by reducing the undesirable effects of the ill-conditioned Hessian matrix. We found that our electrical impedance tomography (EIT) system could produce two-dimensional static images from a physical phantom with 7% spatial resolution at the center and 5% at the periphery.

Static EIT image reconstruction requires a large amount of computation. In order to overcome the limitations on reducing the computation time by algorithmic approaches, we implemented the improved Newton-Raphson algorithm on a parallel computer system and showed that the parallel computation could reduce the computation time from hours to minutes.

INTRODUCTION

In electrical impedance tomography (EIT), we inject currents and measure voltages using electrodes placed on the boundary of a subject. Then, using the boundary current-voltage measurement, we reconstruct a cross-sectional image of resistivity distribution. Webster [4] described various medical and geophysical applications of EIT.

In static impedance imaging, the absolute values of a cross-sectional resistivity distribution are reconstructed. Since current flow is a function of the unknown resistivity distribution, the static impedance imaging problem is nonlinear and requires an iterative algorithm. The modified Newton-Raphson method by Yorkey *et al.* [6] has been suggested as the most sophisticated static image reconstruction algorithm. This method shows good convergence characteristics and reconstructs almost perfect images when no error is involved in the modeling and measurement. However, when modeling error and measurement noise are present and when the number of elements (pixels) is large for good spatial resolution, the performance of this method deteriorates rapidly and produces noisy images. Also when a large number of elements is used, the image reconstruction requires an unreasonably long computation time.

Isaacson [3] and Gisser *et al.* [2] proposed the optimal current injection method where they inject patterns of current through all electrodes. This method improved the quality of static images when combined with the modified Newton-Raphson method. However, due to various sources of error (modeling error, measurement noise, computational error, etc.), static imaging has been tried mostly on computer simulations.

OVERVIEW OF EIT SYSTEM

We have developed a 32-electrode, 12-bit EIT system based on a Macintosh II computer. Figure 1 shows the block diagram of the system. As summarized in Fig. 1, we calculate the optimal patterns of injection currents and use 32 current sources to inject them. For each pattern of injection current, we measure the resulting boundary voltage on the subject using 32 voltage electrodes and a specially designed digital voltmeter. We use the FEM (Finite Element Method) to calculate the boundary voltage of the computer model due to the same injection currents. When we initially assume a certain resistivity distribution for the computer model, the measured voltage and the computed voltage are not the same mainly because of the differences in resistivity distributions. Assuming that the computer model is the correct geometrical representation of the subject including the electrode configuration, we change the resistivity distribution of the computer model until we minimize the error between the measured and computed voltage. This approach for static EIT image reconstruction requires a solution of a nonlinear minimization problem.

Figure 1 shows that the static EIT image reconstruction problem is equivalent to a system identification problem using nonlinear minimization techniques. We can describe the problem in a general sense as follows:

$$\min_{\rho} \max_{c,e} \Phi(\rho ; c ; e) \qquad (1)$$

where $\Phi(\rho ; c ; e)$ is the objective function (error signal) which indicates the difference between the resistivity distribution of the model and that of the subject, ρ is the resistivity distribution of the model, c is the injection current pattern, and e is the electrode configuration. An efficient EIT system requires a measurement method including injection current patterns, electrode size, position, etc. which maximizes the objective function or distinguishability [3]. Given the measurement method, we need an algorithm by which we adjust the resistivity distribution of the model so that the objective function is minimized.

FORWARD SOLVER

In order to solve Eq. (1), we need to solve forward problems. In EIT, the forward problem is to compute boundary voltages or currents of a subject with a certain resistivity distribution due to given injection currents or applied voltages. When we inject current or apply voltage to the thorax, the current-voltage relationship is determined by Poisson's equation with boundary conditions. For a nonhomogeneous, anisotropic and irregularly shaped object such as the thorax, an analytic solution of the equation is impossible. Therefore, we use numerical techniques such as the finite element method

(FEM) or finite difference method (FDM). Since the FEM is advantageous in modeling an arbitrary shaped object, we construct a model of the subject using the FEM.

We have developed a finite element software package including interactive graphical finite element mesh generators and efficient sparse matrix and vector algorithms for solving a sparse linear system of equations. Though this software package is a general purpose finite element analysis tool, we customized the package with special considerations for impedance imaging. Therefore, after we design a finite element mesh including boundary elements and electrode configurations, we can compute boundary voltages or currents for any given resistivity distribution and injection currents or applied voltages.

OPTIMAL MEASUREMENT METHOD

We solve Eq. (1) in two steps. This section is about the Max part of Eq. (1) for which the solution provides the electrode configuration e and the optimal injection current c. Isaacson [3] defined the distinguishability of an injection current pattern c as the ability to distinguish two different resistivity distributions using the boundary voltage measurements. Therefore, the distinguishability d is

$$d = \frac{\| v_1 - v_2 \|}{\| c \|} \tag{2}$$

where v_1 and v_2 are the boundary voltages from resistivity distributions Ω_1 and Ω_2, respectively. In EIT static image reconstruction, we use the error signal which is the difference between the computed voltage from the computer model (solution of a forward problem) and the measured voltage from the subject. Since the error signal is dependent upon the injection current as well as the difference in resistivity distributions between the model and the real subject, we need to study the measurement method in order to maximize the distinguishability or signal-to-noise ratio (SNR).

From the definition of the distinguishability, we can develop algorithms which provide the optimal injection current patterns to maximize the error signal or distinguishability. When we use E electrodes to inject currents into a subject, the maximal distinguishability is achieved by equally spacing large electrodes in the imaging plane and by injecting the optimal current patterns.

We have developed a method to compute all optimal current patterns using Walsh functions and a data synthesis method where boundary voltage values for any injection current patterns are derived from a complete set of boundary voltage measurements using Walsh functions as injection current patterns [5].

NONLINEAR MINIMIZATION METHODS

In order to solve the Min part of Eq. (1), we use a nonlinear minimization algorithm with the resistivity distribution of the computer model ρ as a variable. Therefore, the reconstruction algorithm should change the resistivity distribution of the computer model in a systematic way so that the objective function is minimized.

We assume a FEM model with N nodes, R pixels, E electrodes, and P patterns of injection currents.

Objective function

Given e and c in Eq. (1), we formulate the objective function of our minimization problem as follows:

$$\Phi(\rho) = \frac{1}{p} \sum_{i=1}^{M} w_i r_i^p \tag{3}$$

where p is an even integer, $r_i = f_i(\rho) - v_i$, $M = EP$, and w_i is a weighting function. This is the weighted pth objective function and the minimization problem can be stated as a nonlinear least pth minimization problem. For a given c (injection current pattern), v_i is the ith voltage measurement and $f_i(\rho)$ is the corresponding voltage value computed from the computer model using the FEM.

The objective function is computed by a set of boundary voltage measurements from a subject and another set of boundary voltage values of the computer model which is computed by P repeated solutions of a linear system of equations derived by the FEM.

Computation of the Jacobian and derivative

Yorkey *et al.* [6] described the method of computing the Jacobian matrix $\mathbf{J}$ and the derivative of the objective function $\boldsymbol{g}$ for $p = 2$ and $w_i = 1$ for all i. Here, we derive more general formulas for $\mathbf{J}$ and $\boldsymbol{g}$. From Eq. (3),

$$\boldsymbol{g} = \nabla_\rho \Phi = \mathbf{J}^T \mathbf{W} \boldsymbol{r} \tag{4}$$

where the Jacobian matrix $\mathbf{J}_{mn} = [\nabla_n r_m]$, $\mathbf{W} = \mathrm{diag}(w_1\ w_2\ \ldots\ w_M)$, and the residual vector $\boldsymbol{r} = [r_1\ r_2\ \ldots\ r_M]^T$. Now we define $\tilde{\mathbf{J}} = \mathbf{J}\mathbf{W}^{1/2}$ and $\tilde{\boldsymbol{r}} = \mathbf{W}^{1/2}\boldsymbol{r}$. Then,

$$\boldsymbol{g} = \tilde{\mathbf{J}}^T \tilde{\boldsymbol{r}}. \tag{5}$$

Computation of the Hessian matrix

From Eq. (4), the Hessian matrix is

$$\mathbf{H} = \nabla_\rho (\nabla_\rho \Phi) = \mathbf{J}^T \mathbf{W} \mathbf{J} + \mathbf{M}. \tag{6}$$

In Eq. (6), we ignore the second term $\mathbf{M}$ which contains the residuals and their second derivatives since they are relatively small compared to the first term. Then, the approximate Hessian matrix is

$$\tilde{\mathbf{H}} = \mathbf{J}^T \mathbf{W} \mathbf{J} = \tilde{\mathbf{J}}^T \tilde{\mathbf{J}}. \tag{7}$$

The Ill-conditioning problem

We found that the Jacobian matrix $\tilde{\mathbf{J}}$ and hence the approximate Hessian matrix $\tilde{\mathbf{H}}$ are ill-conditioned for the following reasons.

(A) Crosscorrelation among all pixels

In EIT, all pixel values (resistivities) affect all boundary voltage values. If none of the pixels are correlated, the Hessian matrix would be a diagonal matrix and the steepest descent direction would be the optimal search direction on a circular contour of the objective function. However, crosscorrelations among all pixels skew the contour of the objective function into a narrow hyperellipsoid which indicates a very ill-conditioned Hessian matrix.

(B) Size of model (number of pixels)

We can only use boundary voltage values in EIT, and the sensitivity of the boundary voltage due to each pixel changes greatly depending on the location of the pixel. The boundary voltage is very sensitive to any change in the resistivity value of a pixel (element in a mesh) near the boundary and very insensitive to that of center element. Therefore, this large variation in the sensitivity causes ill-conditioning and requires a careful scaling of the matrix.

Improved Newton–Raphson method

In the modified Newton–Raphson method using the Levenberg–Marquardt method and regularization, the resistivity update at the kth iteration is obtained by solving the following linear system of equations known as the normal equation [1]:

$$\{\tilde{\mathbf{J}}^T \tilde{\mathbf{J}} + (\lambda + \gamma)\mathbf{I}\} \Delta\rho^k = -\boldsymbol{g} = -\tilde{\mathbf{J}}^T \tilde{\boldsymbol{r}}. \tag{8}$$

Then, the new resistivity distribution at the kth iteration is

$$\rho^{k+1} = \rho^k + \Delta\rho^k. \tag{9}$$

However, as we discussed before, $\Delta\rho^k$ is very sensitive to any

noise due to the large condition number of $\tilde{\mathbf{H}}$. Therefore, it is important that we avoid the direct use of the ill-conditioned Hessian matrix..

Eq. (8) can be stated differently as follows:

$$\begin{bmatrix} \alpha\mathbf{I} & \tilde{\mathbf{J}} \\ \tilde{\mathbf{J}}^T & -\nu\mathbf{S} \end{bmatrix} \begin{bmatrix} x \\ \Delta\rho^k \end{bmatrix} = \begin{bmatrix} -\tilde{r} \\ \mathbf{0} \end{bmatrix} \tag{10}$$

where $\alpha\nu = \lambda + \gamma$ and $\mathbf{S} = \text{diag}(\tilde{\mathbf{H}}_{11}\ \tilde{\mathbf{H}}_{22} \ldots \tilde{\mathbf{H}}_{RR})$. Though Eq. (10) is larger than Eq. (8), the augmented matrix is sparse due to two diagonal matrices $\alpha\mathbf{I}$ and $\nu\mathbf{S}$. We solve Eq. (10) using the preconditioned conjugate gradient method.

PARALLEL IMPLEMENTATIONS

On a 16-MHz Macintosh II computer, one iteration of the improved Newton–Raphson method using a mesh with 5% spatial resolution takes about 20 or 30 min using various algorithmic techniques to reduce the computation time.

Computation time using a single processor

Let τ be the total number of nonzeros in the sparse master matrix from the FEM model, then $\tau = O(N^{1+\gamma})$ where $\gamma \approx 0.4$ in most cases [4]. Then, the minimal number of arithmetic operations involved in the sparse LU factorization and substitution are $O(N^{1+2\gamma}) = O(N^{1.8})$ and $O(N^{1+\gamma}) = O(N^{1.4})$, respectively.

In the improved Newton–Raphson method, we do not compute the matrix $\mathbf{H}$ from $\mathbf{J}$ explicitly. Therefore, the total amount of computation for one iteration of the improved Newton–Raphson method is

$$C_{\text{iNR}} \approx O(N^{1.8}) + PR\ O(N^{1.4}) + O((M+R)^2). \tag{11}$$

Parallel computation

We have implemented the improved Newton–Raphson methods on a parallel computer system, the Symmetry from Sequent Computer Systems, Inc., to confirm the feasibility of parallel computations in EIT. The Symmetry system has 20 processors with 256 Mbyte of virtual address space per processor. All processors are tightly coupled and can access shared data structure in memory. We used Sequent parallel C language on the DYNIX operating system.

The computation of the Jacobian matrix $\mathbf{J}$ requires PR times the repeated solutions of a sparse $N \times N$ linear system of equations with different right-hand-sides. Once the matrix is factorized, C processors can start substitution operations simultaneously. Therefore, by using C processors, we can reduce the computation time for computing the Jacobian matrix by a factor of less than $1/C$.

In the improved Newton–Raphson method, we do not compute $\mathbf{H}$ which requires $O((MR)^{3/2})$ computations. And instead of solving the $R \times R$ dense linear system of equations (Eq. (8)) with $O(R^3)$, we solve the $(R+M) \times (R+M)$ sparse linear system of equations (Eq. (10)) using the preconditioned conjugate gradient method which is easily parallelized. Then, the total computation for the improved Newton–Raphson method using C processors is

$$C_{\text{iNR}} \approx O(N^{1.8}) + PR\ O(N^{1.4})/C + O((R+M)^2)/C. \tag{12}$$

Figure 2 shows a reduction in the computation time by using many processors. The results showed a reduction in the computation time within a certain limit as we increase the number of processors. We conclude that the improved Newton–Raphson method is highly parallelizable and the use of parallel computers such as Transputers may solve the computational problems in static impedance imaging.

STATIC IMAGES

Figure 3 shows reconstructed static images from the two-dimensional physical phantom with different sizes of conductors and insulators. We made models of the lung (1200 Ω·cm), heart (150 Ω·cm), spine (2000 Ω·cm), and tissue (300 Ω·cm) by mixing agar powder and NaCl with boiling water. We constructed two models of the human thorax by placing the agar objects in the physical phantom as shown in Fig. 4(a) and (c). Figures 4(b) and (d) show the reconstructed static images of the physical phantom.

CONCLUSIONS

We have developed the improved Newton–Raphson method for static impedance imaging. We implemented the improved Newton–Raphson method on a parallel computer system and showed that parallel computation is very promising in EIT image reconstruction.

Static images reconstructed from a two-dimensional physical phantom showed that we can achieve 5% and 7% spatial resolution at the periphery and at the center, respectively.

REFERENCES

[1] P. E. Gill, W. Murray, and M. H. Wright, *Practical Optimization*, London: Academic Press, 1981.

[2] D. G. Gisser, D. Isaacson, and J. C. Newell, "Current topics in impedance imaging," *Clin. Phys. Physiol. Meas.* vol. **8 Suppl. A**, pp. 39–46, 1987.

[3] D. Isaacson, "Distinguishability of conductivities by electric current computed tomography," *IEEE Trans. Medical Imaging*, vol. **MI-5**, pp. 91–5, 1986.

[4] J. G. Webster (ed.), "Electrical impedance tomography," Adam Hilger, Bristol, England, 1990.

[5] E. J. Woo, R. Pallas-Areny, W. J. Tompkins, and J. G. Webster, "Using Walsh functions in electrical impedance tomography," *Proc. Annu. Int. Conf. IEEE Eng. Med. Biol. Soc.*, vol. **12**, pp. 124–5, 1990.

[6] T. J. Yorkey, J. G. Webster, and W. J. Tompkins, "Comparing reconstruction algorithms for electrical impedance tomography", *IEEE Trans. Biomed. Eng.* **Vol BME-34**, pp. 843–52; 1987.

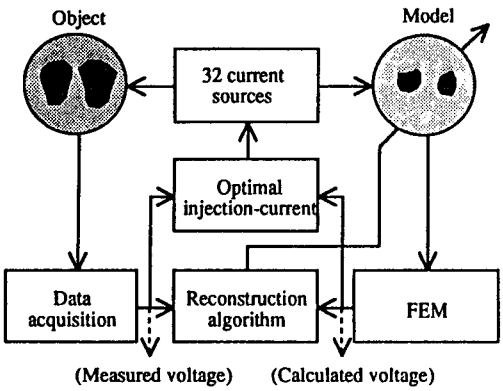

Figure 1 Block diagram of EIT system.

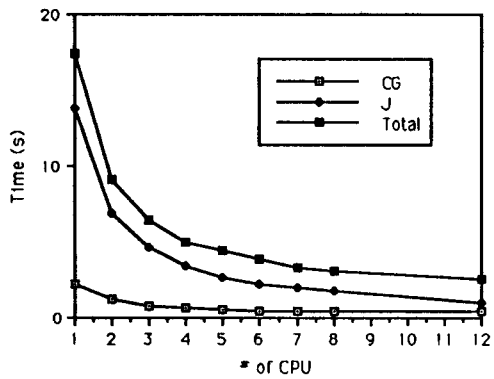

Figure 2 Computation times for a single iteration of the improved Newton–Raphson method. CG is the time for solving Eq. (20) by the conjugate gradient method, J is the time for computing J, and Total is the total computation time.

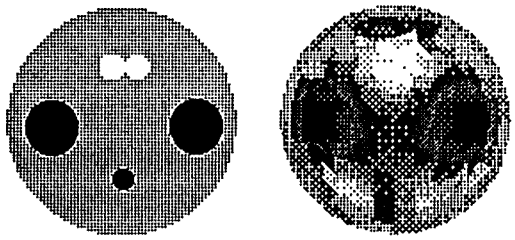

Figure 3 Static images reconstructed from a physical phantom using the improved Newton-Raphson method. (a) True image and (b) reconstructed image.

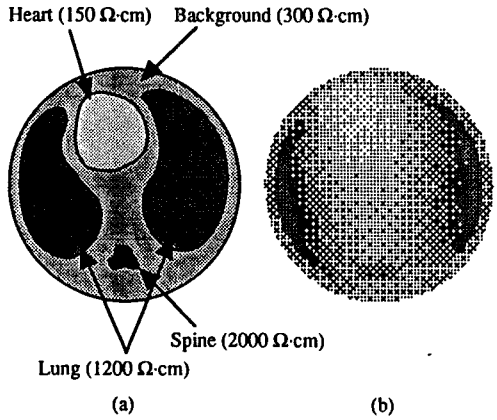

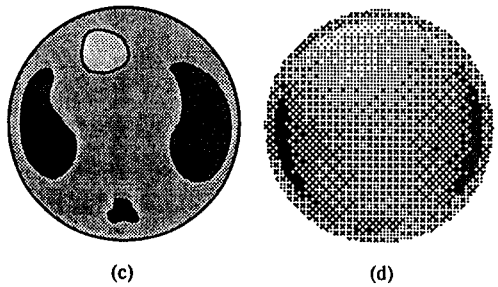

Figure 4 (a) and (c) True images of the physical phantom which model the human thorax using agar objects. (b) and (d) Reconstructed images of (a) and (c), respectively.